Spheroidization of the lamellar microstructure in Ti–6Al–4V alloy during warm deformation and annealing

S. Zherebtsov [a,*], M. Murzinova [b], G. Salishchev [a], S.L. Semiatin [c]

[a] *Laboratory of Bulk Nanostructured Materials, Belgorod State University, Pobeda 85, Belgorod 308015, Russia*
[b] *Institute for Metals Superplasticity Problems, Khalturin 39, Ufa 450001, Russia*
[c] *Air Force Research Laboratory, Materials and Manufacturing Directorate, AFRL/RXLM, Wright-Patterson Air Force Base, OH 45433-7817, USA*

Abstract

The spheroidization behavior of an α colony microstructure in Ti–6Al–4V alloy during warm working and subsequent annealing at 600 and 800 °C was established. The principal features of microstructure evolution were found to be temperature dependent. At 800 °C transformation of the lamellar microstrucuture into a globular one was associated primarily with the classical boundary splitting mechanism followed by further spheroidization of α particles by means of termination migration. For thick α lamellae, however, new grains were formed due to continuous dynamic recrystallization during deformation, but spheroidization per se was limited. A decrease in temperature to 600 °C resulted in increased shear strains, lower diffusivity, and a decrease in the volume fraction of the β phase. Consequently, the thin β interlayers transformed relatively quickly into separate particles while α became the matrix phase. Evolution of the α phase during deformation/annealing at 600 °C was associated with continuous dynamic recrystallization with only limited dynamic or static spheroidization. Static spheroidization kinetics during annealing following warm working were explained in the context of approximate models of boundary splitting and termination migration.

Keywords: Titanium alloy; Thermomechanical processing; Annealing; Microstructure formation; Spheroidization

1. Introduction

Two-phase α/β titanium alloys can exhibit a variety of microstructures, such as that consisting of lamellar α colonies developed during cooling from the high-temperature, single-phase β field. This microstructure has moderate strength and fatigue crack growth resistance but low ductility [1]. In contrast, a microstructure comprising globular α in a matrix of β or transformed β possesses a better balance of strength and ductility and is thus more desirable for many service applications [1].

There are two main mechanisms that may contribute to the spheroidization (or globularization, as it is known in the titanium industry) of lamellar microstructures in titanium alloys during thermomechanical processing (TMP) [2–7]. The first, known broadly as fault migration and/or termination migration, has been used to analyze the diffusional coarsening and spheroidization of lamellar platelets during heat treatment [2,5,6]. The driving force for diffusion is the gradient in chemical potential/solute concentration between the curved edge of a platelet and the flat interphase boundary of a nearby (or the same) platelet; the concentration gradient is typically quantified using the Gibbs–Thompson equation. In such cases, solute atoms diffuse from the edge of the platelet to the flat surface, resulting in a recession of platelet edges and either a general thickening (coarsening) of the plates or the spheroidization of individual lamellae [2,5,8]. Platelet coarsening or spheroidization predominates when the platelet aspect ratio (width/thickness) is large or small, respectively. Not

* Corresponding author. Tel./fax: +7 4722 585416.
E-mail addresses: zherebtsov@bsu.edu.ru, ser_z@mail.ru (S. Zherebtsov).

surprisingly, the kinetics of platelet coarsening or spheroidization in α/β titanium alloys is strongly dependent on the energy associated with the interphase boundaries. In the unworked condition such interfaces have a low energy because of the orientation relationship between the phases and the semi-coherent nature of the boundaries [9,10]. The spheroidization of the lamellar structure can be enhanced significantly by the conversion of the initially semi-coherent boundaries into higher-energy non-coherent ones by hot or warm working in the α/β phase field [11–13].

A second mechanism contributing to spheroidization during TMP consists of the fragmentation of lamellae via the boundary splitting associated with the instability of 90° dihedral angles between interphase α/β boundaries and intraphase α/α boundaries [6,7,14]. Intraphase α/α boundaries may evolve from a recovered substructure, dynamic recrystallization, or the formation of localized shear bands within/across the α lamellae during deformation [6]. Equilibrium between the various surface tension forces at the interphase/intraphase triple junctions leads to a diffusional flux to the interphase surface and the formation of a groove along the α/α boundary. Deepening of the grooves from both sides of an α lamella leads eventually to separate α fragments.

The diffusion of solutes inherent in each of the fragmentation/spheroidization mechanisms underlies the important role of temperature in the kinetic description. The completeness and the rate of spheroidization thus increase with temperature. On the other hand, processing of titanium alloys high in the α/β field may lead to spheroidization and then coarsening of an equiaxed (globular) microstructure which may detract from the strength and fatigue resistance in service [15].

One way to produce and maintain fine α particles is to utilize a low deformation temperature [16]. As shown in Zherebtsov et al. [17], for example, isothermal deformation of Ti–6Al–4V at 550 °C leads to the formation of a homogeneous globular microstructure with a grain/particle size less than 0.5 μm. However, the level of strain necessary to produce a fully spheroidized structure may be rather high. Even at hot working temperatures high in the α/β phase field strains of the order of 2–2.5 are required to yield an almost fully spheroidized microstructure during deformation [18]. With decreasing deformation temperature the strain level required for complete dynamic spheroidization may increase.

The objective of the present work was to establish the possible benefit of using small to moderate warm deformation (e.g. a reduction of 25–70%, equivalent to a true strain of 0.3–1.2) to break down the initial orientation relationship and increase the energy of lamellar interfaces [12] in combination with subsequent static annealing to fragment/spheroidize the lamellar microstructure of two-phase α/β titanium alloys. For this purpose compression and heat treatment experiments were conducted at relatively low (warm processing) temperatures (i.e. 600 and 800 °C) to determine the mechanisms of fragmentation/spheroidization and to estimate the potential of such treatments for the formation of homogeneous ultrafine equiaxed microstructures.

2. Materials and procedures

The program material consisted of the α/β titanium alloy Ti–6Al–4V with a measured composition (wt.%) of 6.3 Al, 4.1 V, 0.18 Fe, 0.03 Si, 0.02 Zr, 0.01 C, 0.18 O and 0.01 N. It was received in the form of a hot rolled 16 mm diameter bar with a β-transus temperature (at which $\alpha + \beta \rightarrow \beta$) of 995 °C. To produce a stable colony microstructure comprising α lamellae within a matrix of β sections of the bar were subjected to a treatment consisting of heating at 955 °C for 15 min, heating to 1010 °C and soaking for 15 min, and furnace cooling to 800 °C and soaking for 20 min. Following the 20 min soak at 800 °C specimens were either water quenched (for subsequent deformation at 800 °C) or controlled furnace cooled (at a rate of 2 °C min^{-1}) to 600 °C, soaked for 2 h, and finally water quenched (for deformation at 600 °C). The measured percentages of β phase were $24 \pm 2\%$ and $18 \pm 1\%$ after water quenching from 800 and 600 °C, respectively.

Cylindrical compression samples measuring 8 mm diameter × 12 mm height were machined from the heat treated bar. Specimens were compressed isothermally in air at 600 or 800 °C in a Schenk mechanical testing system at a nominal strain rate of 10^{-3} s^{-1} to an average true height strain ε of 0.29, 0.69, or 1.2 (corresponding to 25%, 50%, or 70% height reduction, respectively). The local effective strains at the center of the samples (at which all metallographic measurements and observations were made) were larger than the average sample deformation, however [19].

Following compression each specimen was water quenched. To establish static spheroidization behavior, specimens strained to $\varepsilon = 0.29$ or 0.69 were then annealed at the respective deformation temperature for 2, 4, or 8 h (for specimens deformed at 600 °C) or 1, 3, or 6 h (for specimens deformed at 800 °C). To assess long-term behavior selected additional specimens compressed to $\varepsilon = 0.69$ were annealed at 600 °C for 625 h or at 800 °C for 50 h. To avoid oxidation during annealing specimens were placed in evacuated glass capsules. Immediately after annealing each specimen was water quenched.

Following deformation and annealing axial sections were prepared for microstructure determination in the central portion of each specimen using a JEOL JSM-840 scanning electron microscope and a JEOL JEM-2100FX transmission electron microscope. The spheroidized fractions of the α lamellae and plate-like β interlayers were determined based on an aspect ratio $k = l/b < 2$, in which l and b denote the length and thickness, respectively, of remnant lamellae/particles. For this purpose a total area of approximately 0.8 mm^2, lying in the most heavily deformed part of each specimen, was examined for each deformation/heat treatment condition. The error for each measurement was estimated to be less than 10%, with an 80% confidence interval.

3. Results and discussion

Deformation and annealing of Ti–6Al–4V at warm processing temperatures led to the development of various levels of substructure development/recrystallization within the discrete phases, phase fragmentation via boundary splitting, and spheroidization of the remnants of the split lamellae via termination migration. Table 1 summarizes the principal microstructure evolution mechanisms for each temperature and each phase during deformation and during subsequent annealing. For ease of discussion the observations and interpretation of the behavior during deformation are presented first and then the behavior for post-deformation static annealing.

3.1. As-deformed microstructures

The microstructure of the program alloy in the initial condition (after water quenching from 600 °C) consisted of lamellar α colonies within prior β grains (Fig. 1a). The size of the α colonies was ~150 μm, the size of the β grains was ~400 μm, and the thickness of the α lamellae was ~2 μm. The microstructure of specimens cooled to 800 °C prior to water quenching was similar (Fig. 1b) except for the larger fraction of β noted in Section 2.

Stress–strain curves of the alloy compressed at 600 and 800 °C and a nominal strain rate of 10^{-3} s^{-1} exhibited an initial hardening transient, a peak flow stress, and then flow softening (Fig. 1c). Such behavior in single-phase metallic materials is often associated with discontinuous dynamic recrystallization, i.e. the nucleation and growth of new grains [16]. For α/β titanium alloys with a lamellar structure, however, flow softening can be ascribed to rotation of lamellae towards "softer" orientations with low Taylor factors and/or slip transmission across the α/β interfaces [18,20]. A decrease in deformation temperature may increase the extent of each stage due to retardation of the associated kinetic processes.

The main features of microstructure evolution during compression at both 600 and 800 °C comprised an elongation of the β grains and rotation of the α lamellae towards the metal flow direction (Fig. 2). Bent α lamellae and regions of gross localized shear were observed in those α colonies in which the lamellae were close to being parallel to the compression axis. Local bending of lamellae was also frequently observed in the vicinity of colony boundaries due to deformation incompatibility. The localized shearing of lamellae at both deformation temperatures frequently led to fragmentation of the phases (Fig. 2c and d). Those colonies in which the lamellae were initially aligned with the metal flow direction (perpendicular to the compression axis) underwent little morphological change during deformation. The degree of lamellar rotation increased with strain; after $\varepsilon = 1.2$ almost all of the lamellae had become aligned with the metal flow direction at both temperatures.

At the specific deformation temperature of 600 °C the β phase appeared to fragment much more than the α phase. In fact, after the smallest imposed strain ($\varepsilon = 0.29$) some of the β layers had split into plates of various lengths. As shown in the insert in Fig. 2a, division of the β phase may be associated with local shear deformation (A), boundary splitting (B), and possibly local dissolution (C). Local dissolution can be rationalized as a result of the observed decrease in the percentage of β phase during deformation from the initial value of $18 \pm 1\%$ to $15 \pm 2\%$ after $\varepsilon = 1.2$.

Gaps between the segments of the fragmented β layers measuring up to a few micrometers enabled the flow of adjacent α lamellae towards each other. The length of the gaps increased with strain, eventually resulting in the formation of a microstructure which can be qualitatively described as comprising β particles within an α matrix (Fig. 2e). The decrease in the length of the β plates did not lead to an increase in their thickness, however, the number of the β particles increased, resulting in microstructure refinement (Fig. 2a, c and e).

Fragmentation and spheroidization of the α phase during deformation at 600 °C is more difficult to discern, partially due to its large volume fraction. In many cases the bending of adjacent β layers towards each other resulted in pinch-off of the α lamellae lying between them (Fig. 2a and c). The process of penetration of the β phase along the boundaries formed within the α lamellae, which is typical for high-temperature deformation of such alloys, was

Table 1
Microstructure evolution mechanisms operating during deformation and subsequent annealing of Ti–6Al–4V at 600 and 800 °C.[a]

Microstructure evolution mechanism	600 °C				800 °C			
	Deformation		Annealing		Deformation		Annealing	
	α	β	α	β	α	β	α	β
Macroscopic shearing/bending	+	+	–	–	+	+	–	–
α Lamellae pinch-off due to local bending	+	–	–	–	–	–	–	–
Continuous dynamic recrystallization	+	+	–	–	+	+	–	–
Continuous static recrystallization	–	–	+	–	–	–	+	±
Platelet local shear deformation	+	+	–	–	±	–	–	–
Platelet partial dissolution	–	+	–	+	–	–	–	–
Platelet fragmentation via boundary splitting	±	+	±	+	+	+	+	+
Spheroidization of platelets via termination migration	–	–	–	±	+	+	+	+

[a] Ratings: +, very common; ±, sporadic/limited; –, not observed.

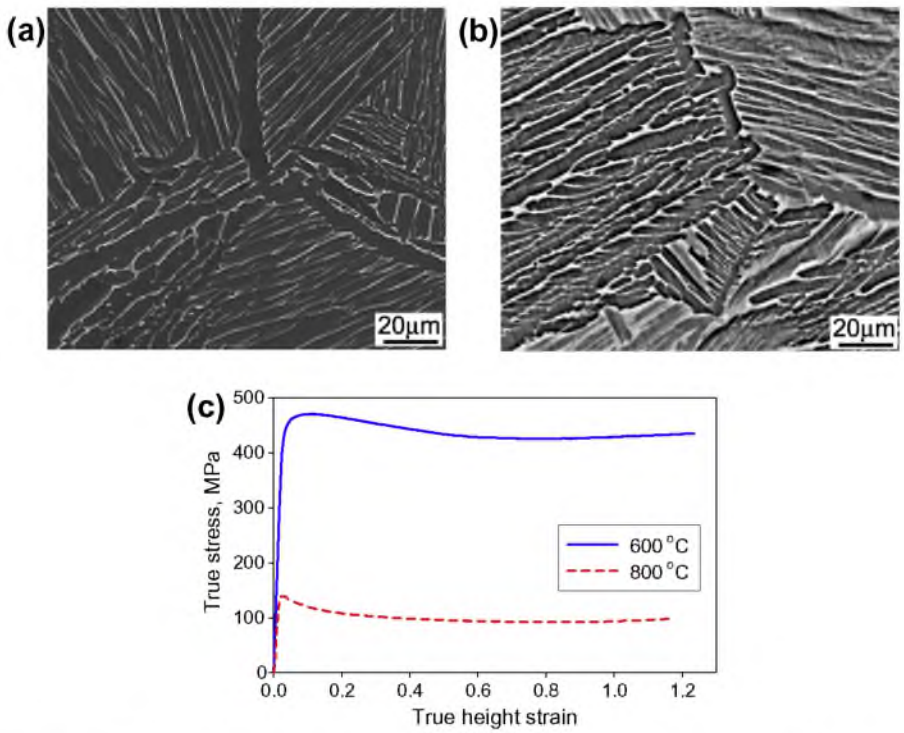

Fig. 1. (a and b) SEM micrographs of the initial microstructure of the Ti–6Al–4V alloy and (c) flow curves obtained during deformation at 600 and 800 °C and a nominal strain rate of 10^{-3} s^{-1}. (a and b) α is the darker phase, β is the lighter phase.

rather sporadic and thus cannot be considered as the main process of microstructure evolution for the α phase.

During deformation at 800 °C microstructure evolution was found to be mainly associated with the common processes of α platelet pinch-off/fragmentation via boundary grooving (Fig. 2b) and subsequent spheroidization of the remnant lamellae by termination migration (Fig. 2d and f). After a height strain $\varepsilon = 1.2$ a mixed microstructure (comprising remnants of lamellae along the metal flow direction and globular α particles) was formed (Fig. 2f). The size of the α particles was ~1.5 μm. In contrast to deformation at 600 °C, the percentage of β phase increased ($24 \pm 2\%$ in the initial condition and $27 \pm 2\%$ after $\varepsilon = 1.2$), and the β phase remained as the matrix during deformation at 800 °C.

Microstructure evolution during deformation was further elucidated by transmission electron microscopy (TEM) (Figs. 3 and 4 for deformation at 600 and 800 °C, respectively). The initial microstructure consisted of α lamellae separated by thin laths of the β matrix (Figs. 3a and 4a). The dislocation density in the α phase was low, with only individual dislocations being observed. In the β phase, thin laths of martensitic α were noted.

At 600 °C the dislocation density in the α phase increased considerably after an average height strain ε of only 0.29 (Fig. 3b). Dislocation walls/pile-ups formed in some of the α lamellae. Sporadic offsets in the interphase boundary (indicated by the triangle in Fig. 3b) implied some degree of slip transmission across the α/β interface [21]. In the β phase grooves were sometimes seen at those points at which transverse β/β boundaries met the α/β interface (indicated by the arrows in Fig. 3c). The observed grooving appears to underlie a boundary splitting process that leads to fragmentation of the β layers and the formation of discrete β particles. After a strain $\varepsilon = 0.69$ substructure comprising a high dislocation density and subgrains with a size of 200–500 nm suggestive of continuous dynamic recrystallization (CDRX) were found in the majority of the α lamellae. In addition, localized deformation bands with a spacing of 0.5–1 μm were observed in some α lamellae, especially those that were relatively thick (~4 μm) (Fig. 3d), suggesting a mechanism of fragmentation of the thick lamellae. The intense localized shear deformation in thick α lamella was suppressed/terminated in the adjacent β phase and hence not transmitted to the next α lamella (Fig. 3d). Termination of the shear deformation in the β phase was likely a result of its lower strength and higher ductility in comparison with the α phase at this temperature.

An increase in strain to $\varepsilon = 1.2$ resulted in the formation of a mixed lamellar/globular microstructure at 600 °C. The boundaries between the remnants of the α lamellae and the β layers (Fig. 3e, with the location of the former β layers shown by arrows) were difficult to discern. The β phase had broken into separate fragments and could not be considered the matrix phase, as noted above. A very high dislocation density and subgrain structure were observed within the α phase. The size of the subgrains within the α phase and the β fragments was 200–500 nm. In some places a homogeneous microstructure with relatively equiaxed

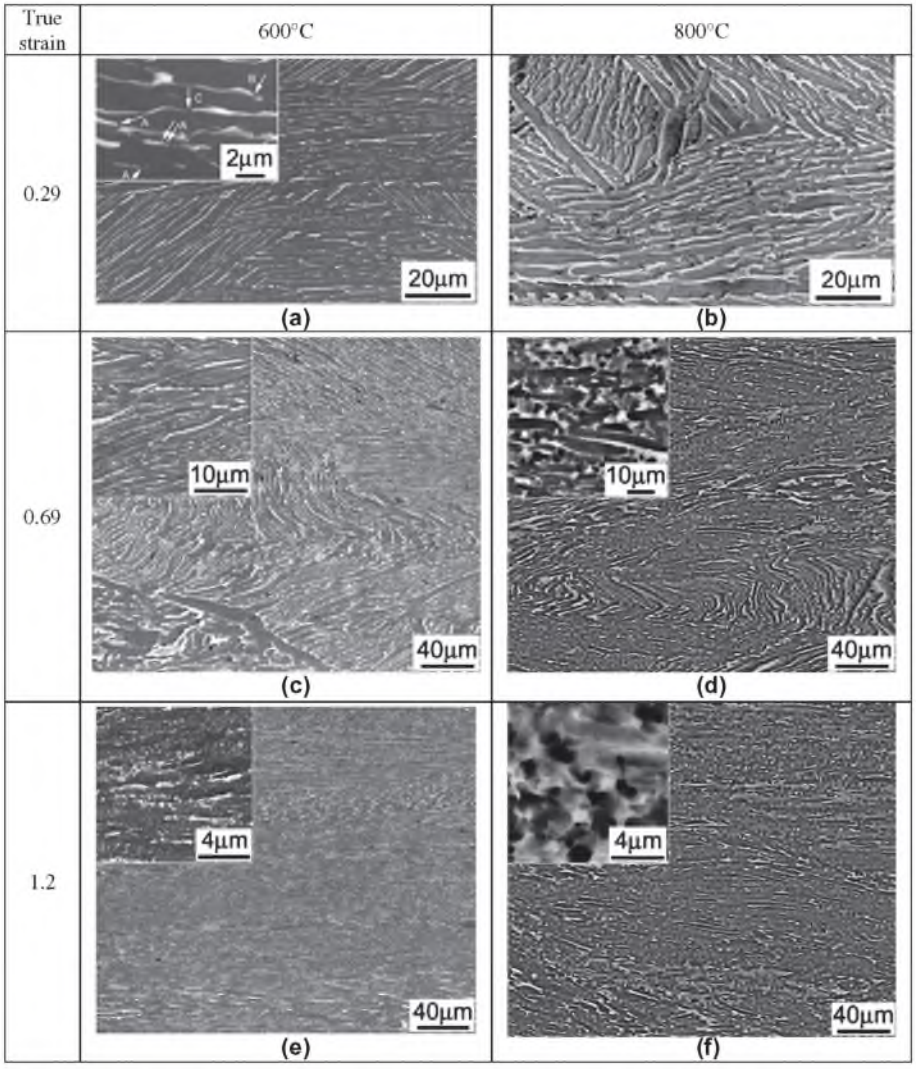

Fig. 2. SEM micrographs of Ti–6Al–4V alloy following compression at (a, c, e) 600 °C or (b, d, f) 800 °C and a nominal strain rate of 10^{-3} s^{-1} to a true average height strain of (a and b) 0.29, (c and d) 0.69, or (e and f) 1.2. The compression axis is vertical in all micrographs.

300–400 nm fragments without any sign of remnant lamellae was observed (Fig. 3f).

At the higher deformation temperature (800 °C) the character of microstructure evolution was somewhat different. After a height strain $\varepsilon = 0.29$ some α and β laths were bent and the dislocation density in the α phase increased relative to that for the initial condition (Fig. 4b). Moreover, subgrains with an irregular shape and curved boundaries were seen in the α phase. In the β phase only separate dislocations (or loose arrays of dislocations) and fine α lamellae were observed. After $\varepsilon = 0.69$ the microstructure was markedly changed. Although a lamellar microstructure still remained in some places, a number of the α lamellae contained low- and high-angle boundaries (Fig. 4c). In some cases the boundaries showed a fringe contrast, implying a perfect structure. After $\varepsilon = 1.2$ at 800 °C lamellae of the α phase were partially recrystallized with a mean α grain size of 1.3 μm (Fig. 4d). The α grains had a low to moderate dislocation density and slightly curved boundaries with a fringe contrast. The dihedral angles at the triple junctions were close to equilibrium (i.e. ~120°). The β layers were also divided into separate subgrains by transverse boundaries. Grooves of various depths were observed at the interphase boundaries of the β layers. In some places the β layers had transformed into almost globular particles with perfect boundaries.

A number of aspects of the dynamic microstructure evolution in the α and β phases at both 600 and 800 °C were typical of CDRX often seen in single-phase alloys [16]. The steady-state flow stages of the stress–strain curves of the program alloy (Fig. 1c) are possibly related to this recrystallization process. However, in the case of two-phase titanium alloys with a lamellar microstructure recrystallization within each phase is only the first step in spheroidization. One of the effects of CDRX is the formation of unstable triple points formed by the interphase and α/α or β/β boundaries. Subsequent lamellar fragmentation occurs by the grooving/boundary splitting mechanism. In the present work such a two-stage process appears to be applicable for the β layers. CDRX also appears to play

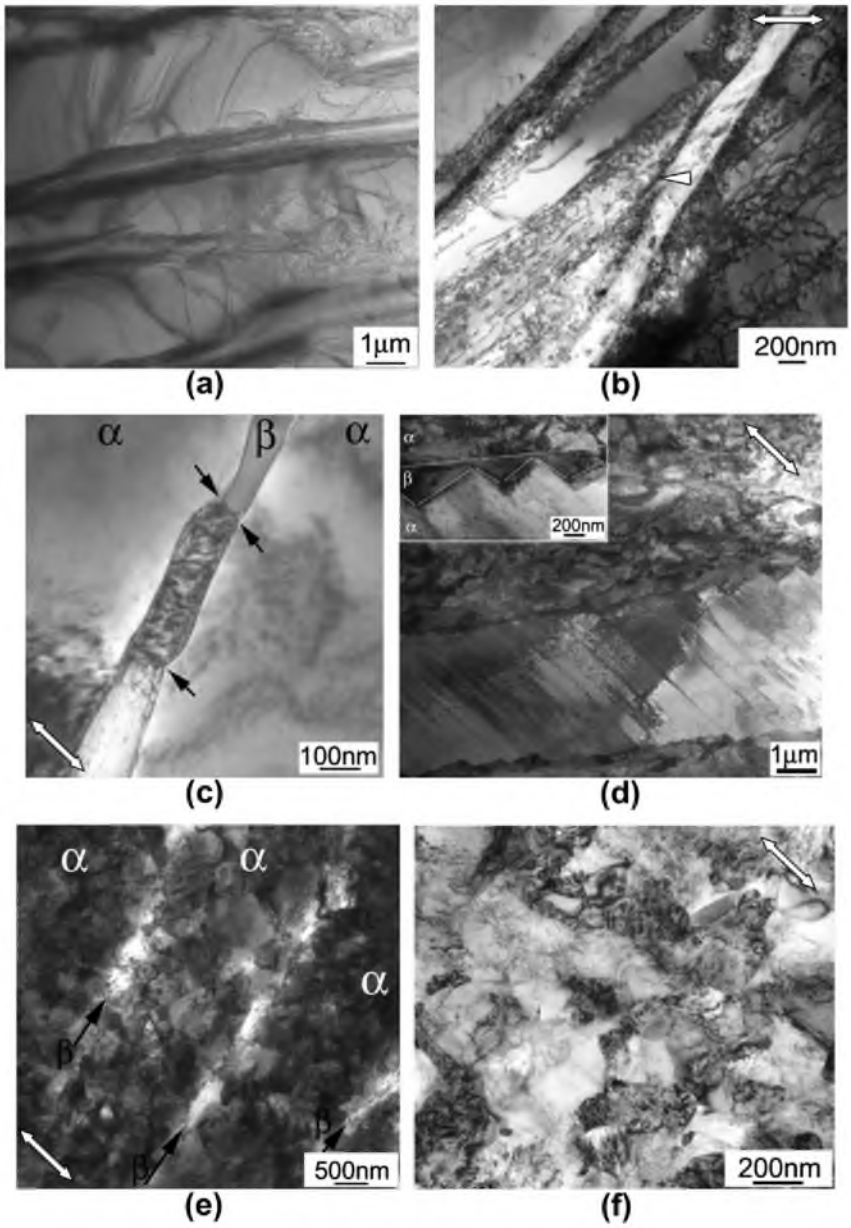

Fig. 3. Bright field TEM images of microstructure developed in Ti–6Al–4V alloy during deformation at 600 °C: (a) initial microstructure and after height strains of (b and c) 0.29, (d) 0.69, and (e and f) 1.2. The compression axis is indicated by the arrow in each micrograph. The triangle in (b) indicates an offset at the α/β interface.

an important role for the α lamellae at both deformation temperatures (Figs. 3e, f and 4c, d). Furthermore, α lamellae appeared to be divided somewhat due to boundary splitting at 800 °C (inset in Fig. 2d), however, a decrease in temperature to 600 °C noticeably attenuated the contribution of boundary splitting to the α lamella fragmentation process.

The main factor inhibiting dynamic fragmentation of the α phase via boundary splitting is most likely related to the greater thickness of the α lamellae. Being much thinner, the β layers much more readily divide into separate fragments by boundary splitting along transverse boundaries. Since the size of the resulting β particles is of the same order of magnitude as the original β layer thickness, the α phase may indeed penetrate along the boundaries developed in the β phase, thereby segmenting the matrix phase. In contrast, the thickness of the α lamellae are at least four times as large as the subgrains observed during the final stage of deformation, thus suggesting that the microstructure refinement is primarily associated with CDRX [16] and, to a limited extent, with localized shear at 600 °C.

3.2. Dynamic spheroidization behavior and kinetics

A quantitative evaluation of the microstructure changes indicated that most of the rotation of α lamellae with respect to the compression axis occurred during the initial

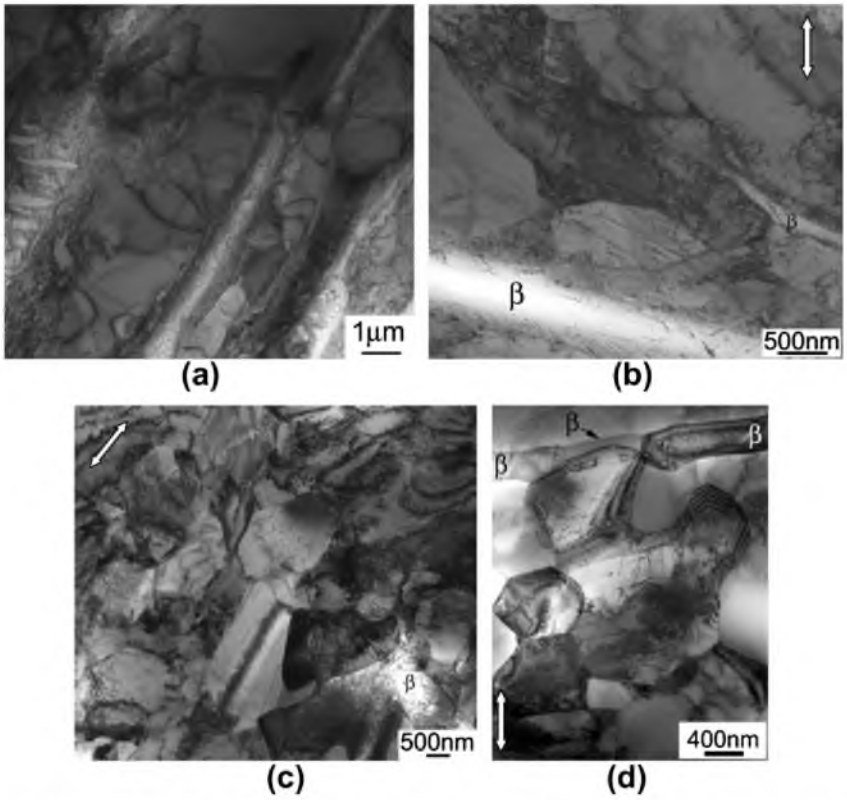

Fig. 4. Bright field TEM images of microstructure developed in Ti–6Al–4V alloy during deformation at 800 °C: (a) initial microstructure and after height strains of (b) 0.29, (c) 0.69, and (d) 1.2. The compression axis is indicated by the arrow in each micrograph.

stages of deformation ($\varepsilon = 0$–0.69). The inclination of the lamellae relative to the metal flow direction saturated at an angle ~10° at 600 °C and ~17° at 800 °C (Fig. 5a). The slightly greater rotation of lamellae at 600 °C may be associated with the reduced rate of dynamic recovery and greater contribution of dislocation glide/multiplication to the accommodation of the imposed deformation. In addition, the flow softening at both temperatures (Fig. 1c) occurred at strains exhibiting the highest rate of lamellae rotation ($\varepsilon \leqslant 0.3$, approximately), while the formation of new grains/particles was observed only at $\varepsilon \geqslant 0.69$ (Figs. 2–4). Consequently, softening of two-phase titanium alloys with a lamellar microstructure in the early stages of deformation may indeed be hypothesized as due to (a) the rotation of lamellae towards "softer" orientations with low Taylor factors and (b) features associated with the evolution of dislocation substructure.

The dependence of the fraction of globular particles with an aspect ratio $k = l/b \leqslant 2$ on strain exhibited a different relationship (Fig. 5b). At $\varepsilon \leqslant 0.69$ the fraction of globular particles was relatively small. Above $\varepsilon \approx 0.69$ it increased rather rapidly. In addition, the rate of dynamic spheroidization increased measurably with temperature.

The observed decrease in the length of α lamellae and β layers, metrics of the fragmentation/spheroidization processes, showed three distinct stages (Fig. 6a and b): (a) a

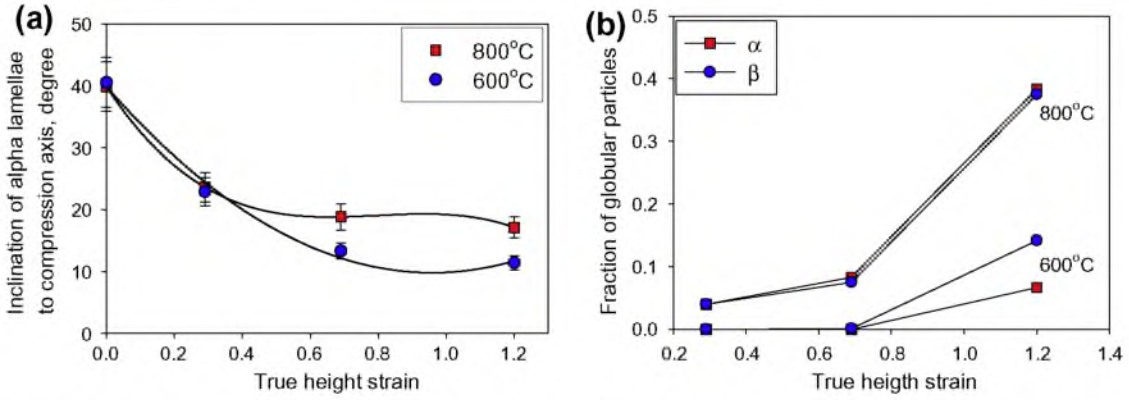

Fig. 5. (a) Inclination of α lamellae to the metal flow direction and (b) fraction of globular particles (with aspect ratio $k \leqslant 2$) (b) as a function of strain for Ti–6Al–4V alloy deformed at 600 and 800 °C.

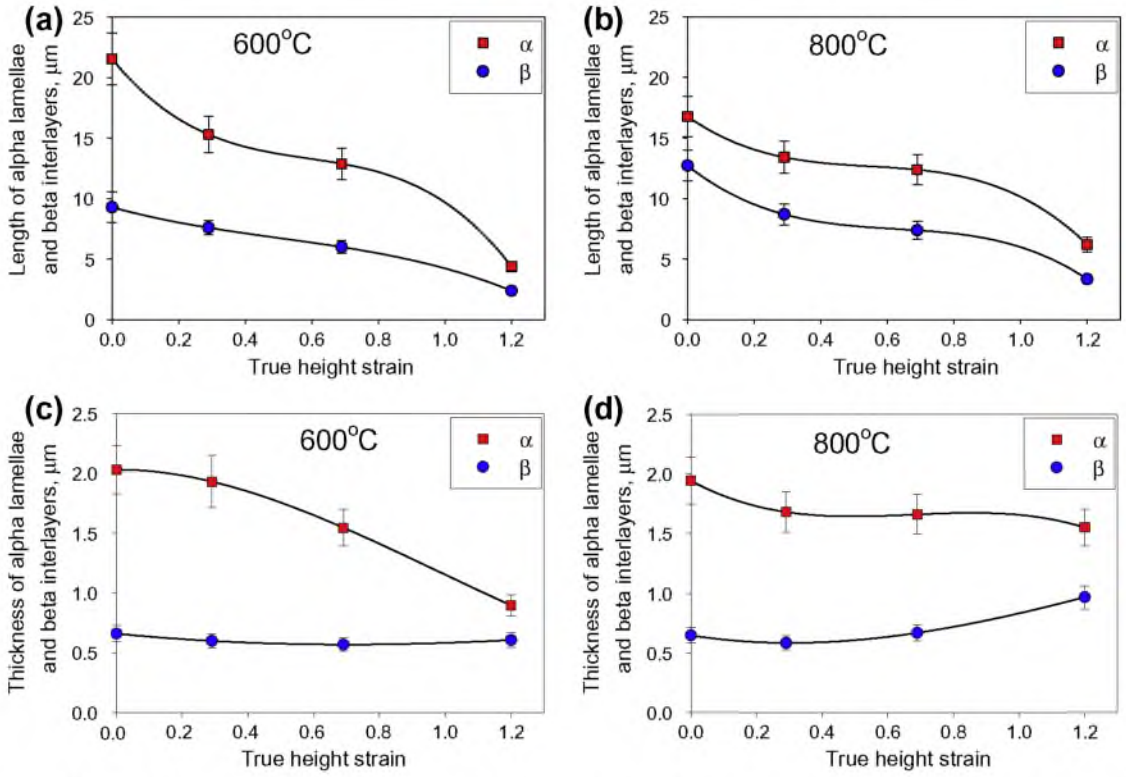

Fig. 6. Length (a and b) and thickness (c and d) of α lamellae and β layers as a function of strain for Ti–6Al–4V alloy deformed at (a and c) 600 °C and (b and d) 800 °C.

sharp decrease from $\varepsilon = 0$ to $\varepsilon = 0.29$; (b) a retardation of the process up to $\varepsilon = 0.69$; (c) another rapid decrease in the length at yet larger deformation. The formation of shorter lamellae during the first stage was probably associated with the development of localized shear deformation within some colonies. During the second stage dislocations were rearranged into walls and sub-boundaries. This process was accompanied by a decrease in flow stress (Fig. 1c) and a small change in the length of lamellae and fraction of globular particles (Figs. 5b and 6a, b). Finally, during the third stage a pronounced decrease in the length of lamellae, as well as an increase in the fraction of globular particles, due to substantial dynamic fragmentation/spheroidization was observed. It should be noted that the last two stages were not accompanied by work hardening at either temperature (Fig. 1c). This implies the occurrence of a dynamic restorative process, such as recovery or recrystallization (which maintains an approximately constant dislocation density) or the beginning of superplastic flow associated with an increase in new interphase/grain boundaries [16,17].

Quantitative microstructure measurements also revealed considerable changes in the thickness of the α lamellae during deformation (Fig. 6c and d). For example, the thickness of α lamellae decreased by a factor of 2 (from 2 to 0.9 μm) after $\varepsilon = 1.2$ at 600 °C (Fig. 6c). Concurrently the thickness of the β layers underwent almost no change for this reduction and temperature. At 800 °C the thickness of the α lamellae decreased slightly, while the thickness of the β layers tended to increase (Fig. 6d).

At first glance the thickness measurements appear unusual with respect to those predicted on the basis of homogeneous, constant volume compressive deformation of metals. For an equiaxed grain with an initial size (diameter) d_o, the instantaneous axial dimension d should vary as $d = d_o \exp(-\varepsilon)$. Taking d and d_o as the final and the initial thickness of an α lamella lying perpendicular to the compression axis from the onset of deformation, respectively, a strain $\varepsilon = 1.2$ at 600 °C would reduce the platelet thickness from ~2 μm to ~0.6 μm, which is ~30% less than the measured value in Fig. 6c (i.e. 0.9 μm). However, the measurements in Fig. 6c and d pertain to averages for all lamellae, most of which lie at an angle to the metal flow direction at the beginning of deformation. Hence, the normal strains (and lamella thinning) in coordinate systems rotated to various angles to the compression axis would be less than this.

Two additional factors, one associated with stereology and the other with the strain state itself, mitigate such a simple analysis of platelet thinning. First, a two-dimensional section does not give the true thickness of a lamella lying at an arbitrary angle to the plane of such a section [22,23]. At small strains this angle may be quite large, and the apparent thickness will be large as well. On the other hand, large strains tend to rotate the lamellae to coincidence with a plane normal to the compression axis

(Fig. 5a). In such instances the lamellae are close to normal to the section plane, and an axial section does yield a reasonable approximation of the actual platelet thickness. With regard to the second factor, relatively little is known about the micro-mechanisms of the deformation of lamellar microstructures, especially near the phase interface. Because of the large difference in flow stress of the α and β phases in two-phase titanium alloys it is likely that deformation is not the same in both phases and comprises some element of interfacial shear, in addition to normal strains, even for lamellae oriented perpendicular to the compression axis. Interfacial shear probably plays a key role in the loss of coherency between the α and β phases during warm and hot working [12]. An analysis of such local strains warrants future research.

3.3. Microstructure evolution during annealing

The microstructures of specimens deformed to $\varepsilon = 0.29$ and 0.69 at 600 °C and then annealed for short times ($\leqslant$8 h) at the same temperature were very similar to their as-deformed counterparts (e.g. Figs. 2c and 7a). Annealing of specimens deformed at 800 °C for 1, 3 and 6 h at the deformation temperature resulted in higher levels of spheroidization and, concurrently, an apparent thickening of the remnants of the lamellae (Figs. 2d and 7b). Grooves dividing lamellae into separate particles were observed at the α/β interfaces.

Substantially longer time annealing at 600 and 800 °C resulted in dramatic microstructure changes (Fig. 7c and d). After annealing at 600 °C for 625 h, for example, the β phase was almost completely spheroidized into chains of small particles (~1 μm) along α lamellae (Fig. 7c). The α phase took on the appearance of the matrix phase but still exhibited a somewhat lamellar morphology, however, grains ~0.3 μm in size were observed within the α phase. Long time annealing at 800 °C led to noticeable spheroidization of the α phase (Fig. 7d). The β phase was found in the spaces between the α particles and appeared to be constrained to narrow channels between such particles. The shape of the β particles was thus close to plate-like rather than globular.

The fraction of β phase after annealing at 600 °C for 625 h decreased to 10 ± 1% from 18 ± 1% (initial condition) and 15 ± 2% (as-deformed condition), thereby suggesting a slow approach to equilibrium at 600 °C. An evaluation of the phase fractions in specimens after deformation and long time annealing at 800 °C revealed approximately the same β volume fraction (24 ± 2%) as in the initial and as-deformed conditions. The β phase volume fractions noted in the present work are similar to those reported previously [24,25] for Ti–6Al–4V materials with a similar composition, i.e. ~6% at 650 °C and ~19–27% at 815 °C. It should also be noted that after long time annealing at either 600 or 800 °C the β phase did not form a continuous network (Fig. 7c and d), apparently due to its low volume fraction. More specifically, the α particles were mostly surrounded by β phase following long time annealing at 800 °C (Fig. 7d), whereas at 600 °C the α phase was the matrix, with relatively homogeneously distributed globular β particles (Fig. 7c).

TEM revealed only minor microstructure changes after annealing at 600 °C for 2–8 h (Fig. 8a). In specimens deformed at 800 °C to $\varepsilon = 0.69$ and then annealed at 800 °C for 6 h the dislocation substructure became rearranged into dislocation walls and sub-boundaries, while the overall dislocation density decreased considerably (Fig. 8d and e). Grain and interphase boundaries become straight. In addition, the interphase boundaries at the triple junctions with grain boundaries did not exhibit a noticeable curvature (Fig. 8e), unlike the grooving observed by SEM (Fig. 7b). This may be due to the relatively low energy associated with low angle grain boundaries. As discussed by Mullins [7,26], the groove angle (δ) satisfies the equilibrium equation for the surface tensions associated

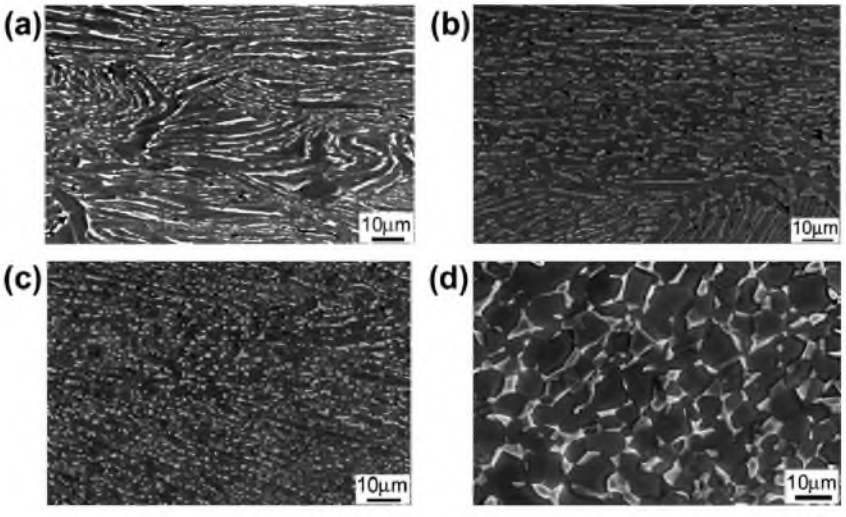

Fig. 7. SEM micrographs of Ti–6Al–4V alloy compressed and then annealed at (a and c) 600 and (b and d) 800 °C. The annealing time was 8 (a), 6 (b), 625 (c) or 50 h (d). The true height strain before annealing was $\varepsilon = 0.69$.

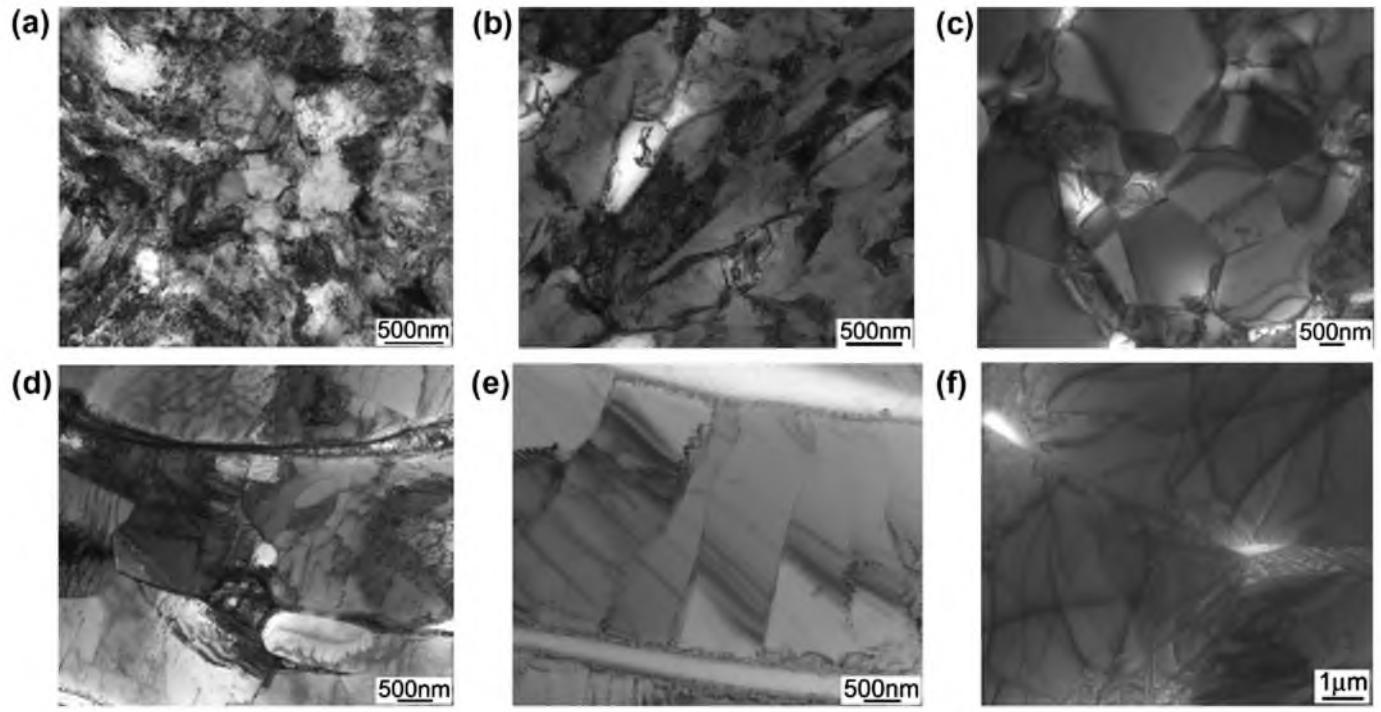

Fig. 8. TEM micrographs of Ti–6Al–4V alloy after compression and annealing at 600 (a–c) and 800 °C (d–f) for 8 (a), 625 (b and c), 6 (d and e) or 50 h (f). The true height strain before annealing was $\varepsilon = 0.69$.

with the surface energy of the α/β interface ($\gamma_{\alpha\beta}$) and the α/α boundary ($\gamma_{\alpha\alpha}$) within the α lamellae, i.e. $\sin\delta = \gamma_{\alpha\alpha}/2\gamma_{\alpha\beta}$. The energy of low angle dislocation boundaries comprises that of constituent dislocations [27] and is proportional to the misorientation: $\gamma_{\alpha\alpha} \sim \theta$. Hence, noticeable grooving cannot be expected for those boundaries which have low misorientation after a long annealing time.

Long time annealing at 600 °C for 625 h resulted in considerable modification of the microstructure. The dislocation density decreased and the boundaries between grains/fragments became thinner (Fig. 8b). In some areas a recrystallized microstructure with a grain size of ~2–3 μm was observed (Fig. 8c). In the case of long time annealing at 800 °C the microstructure consisted of very large dislocation-free particles of the α phase (Fig. 8f). The dihedral angles at the triple junctions were close to 120°. Discrete particles of the β phase (with an elongated triangular shape) were located between α particles at their boundaries or triple junctions.

3.4. Static spheroidization behavior and kinetics

Further fragmentation/spheroidization during annealing following deformation was found to occur in several stages, as shown in Fig. 9. In this figure the arrows indicate the fractions of dynamically spheroidized phase from Fig. 5b. During the first stage of annealing (~1–3 h) the fraction of globular particles increased rather rapidly at both temperatures. During annealing for 8–10 h the rate of spheroidization decreased, in some cases almost to 0. However, long-term annealing of specimens compressed to $\varepsilon = 0.69$ at both temperatures led to an increase in spheroidization rate. Such a complex behavior may be related to the various processes occurring during static spheroidization, as noted in Stefansson and Semiatin [3] and Semiatin et al. [5], i.e. boundary splitting due to thermal grooving at short times and termination migration at long times. Boundary splitting is more important during the early stages of annealing, during which the β/β and/or α/α grain boundaries have high misorientations (whose values are dependent on prior strain) and hence sufficient boundary energy to drive the grooving process. With prolonged exposure the boundary energy may decrease, thus slowing down boundary splitting. Concurrent recovery within the matrix through which solutes diffuse may also decrease the diffusivity/rate of diffusion, thereby decreasing the rate of fragmentation/spheroidization due to boundary splitting. On the other hand, at long times static spheroidization due to mass (solute) transport from the ends/edges of remnant lamellae to the flat (or nearly flat) faces of an adjacent (or the same) lamella and perhaps some degree of static coarsening by Ostwald ripening provide effective means for the formation and subsequent coarsening of globular particles.

With respect to the effect of imposed strain on kinetics, the extent of spheroidization during annealing increased with prior strain (Fig. 9), a trend similar to previous observations for Ti–6Al–4V deformed and annealed at hot working temperatures [19]. Relatively slow static spheroidization was found during annealing at 600 °C; only ~6 and 11% globular particles were observed after annealing for 8 h following $\varepsilon = 0.29$ and 0.69, respectively. At 800 °C the level of static spheroidization was much higher, for

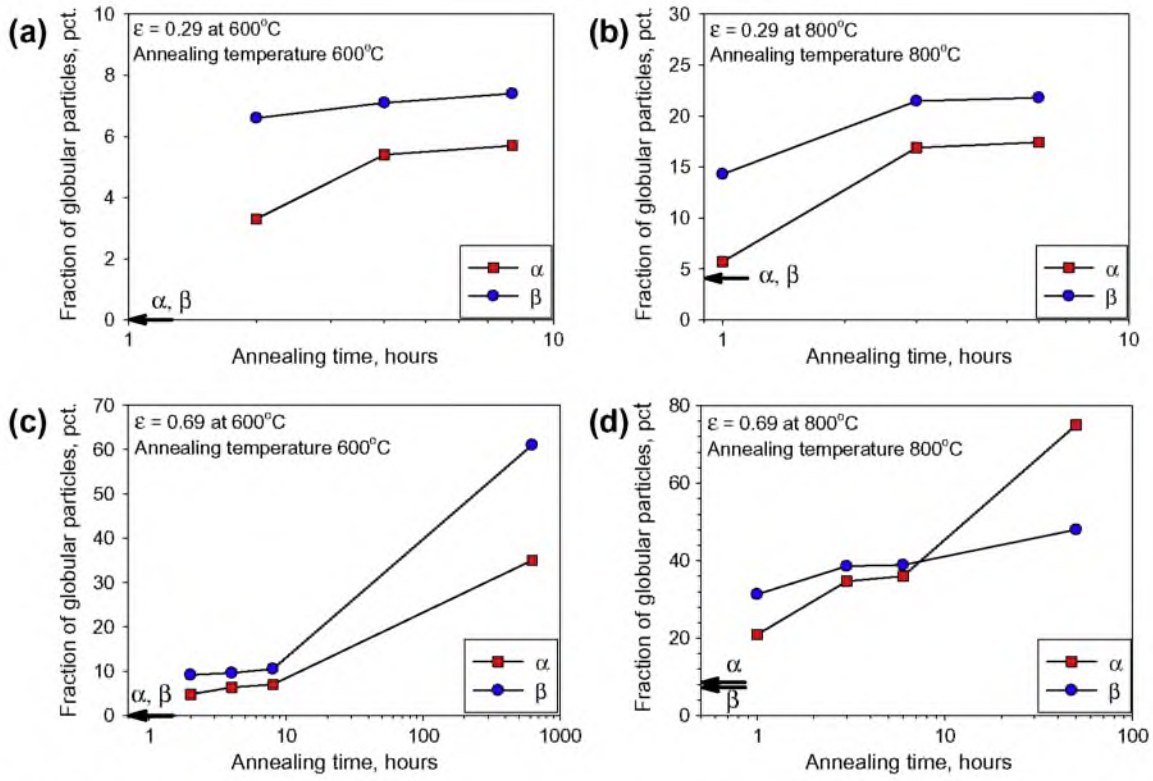

Fig. 9. Static spheroidization measurements for Ti–6Al–4V alloy warm worked and annealed at (a and c) 600 or (b and d) 800 °C. The imposed true height strains prior to annealing were (a and b) 0.29 and (c and d) 0.69. The arrows indicate the fraction of globular α and β particles in the as-deformed condition from Fig. 5b.

example 35–40% of the microstructure was globular after $\varepsilon = 0.69$ and annealing for 6 h. At both temperatures the β phase spheroidized noticeably faster than the α phase because of the difference in thickness, as discussed above.

It is important to note that deformation to $\varepsilon = 0.69$ at both 600 and 800 °C followed by annealing for 3–6 h gave approximately the same amount of spheroidized microstructure as deformation to $\varepsilon = 1.2$ at the same temperatures without subsequent annealing (Fig. 5b vs. Fig. 9c and d). However, not surprisingly, a much finer structure was developed in the latter case, i.e. via dynamic spheroidization.

3.5. Analysis of static spheroidization kinetics

Some of the observations of static spheroidization behavior were interpreted in terms of the boundary grooving and termination migration models previously developed and validated for Ti–6Al–4V deformed and heat treated at hot working temperatures [6].

3.5.1. α Platelet pinch-off/fragmentation via boundary grooving

Penetration of the β phase along the deformation-induced boundaries formed within α lamellae (and vice versa) was analyzed using the Mullins model [7,26]. In the case of penetration of α lamellae the time t_p to complete the grooving process is given by [6,26]:

$$t_p = 0.2(d_\alpha)^3 \Big/ A(m_g)^3, \tag{1}$$

in which d_α is the thickness of the α lamella and m_g represents the average slope at the root of the triple point [3].

The coefficient A in Eq. (1) is given by the equation [6]:

$$A = C_\beta \gamma_{\alpha\beta} V_M D_\beta / R_g T, \tag{2}$$

in which C_β denotes the equilibrium concentration (in terms of atomic fraction) of the rate-limiting solute in the β phase, $\gamma_{\alpha\beta}$ is the α/β interface energy, V_M is the molar volume of the α platelet material, D_β is the diffusivity of the rate-limiting solute through the β matrix, R_g is the universal gas constant, and T is the absolute temperature (in K).

Because neither the α nor the β phase in Ti–6Al–4V is a terminal solid solution, the term C_β in Eq. (2) should be replaced by the composition factor C_F [6,28]:

$$C_F = C_\beta(1 - C_\beta)/(C_\alpha - C_\beta)^2[1 + \partial \ln r / \partial \ln C_\beta], \tag{3}$$

Here, C_α is the concentration of the rate-limiting solute in the α phase and the term $[1 + \partial \ln r / \partial \ln C_\beta]$ is a thermodynamic factor ($r \equiv$ activity coefficient of the solute in the β phase). This composition factor correction is particularly important for alloys such as Ti–6Al–4V alloy in which there is only a small composition difference, $C_\beta - C_\alpha$, between the phases, thus leading to a large acceleration of the interfacial energy driven process [28].

Input data required to calculate the time to complete the boundary grooving process comprise the slope $m_g \approx 0.35$, the molar volume of the α platelet material $V_M = 10{,}440\ \text{mm}^3$, and the α/β surface energy, taken here to be $\gamma_{\alpha\beta} = 0.26\ \text{J m}^{-2}$, as per Weiss et al. [14]. The α lamella thickness d_α was equal to ~1.5 μm at 600 °C or ~1.6 μm at 800 °C (Fig. 6c,d). As shown in Semiatin et al. [29], the diffusion of vanadium through the β matrix is rate limiting in comparison with the diffusion of aluminum. The thermodynamic factor for vanadium solutes in β titanium is equal to ~1 [30]. Based on the data reported in Semiatin et al. [29] and Sargent et al. [25], the composition term (i.e. $C_\beta\,(1 - C_\beta)/(C_\alpha - C_\beta)^2$) at 600 and 800 °C is equal to approximately 6 and 14, respectively. The measured diffusivities of vanadium in the β phase were calculated from the expression [29]:

$$D_v^\beta\ (\mu\text{m}^2\ \text{s}^{-1}) = 77{,}000 \exp(-17{,}460/T\ (\text{K})), \tag{4}$$

thus yielding diffusivities of 0.00016 and 0.0065 $\mu\text{m}^2\ \text{s}^{-1}$ at 600 °C and 800 °C, respectively.

Substituting the values of the various material and geometry parameters into Eqs. (1)–(3) gives the time necessary to complete the boundary grooving process as ~9750 and ~190 h at 600 and 800 °C, respectively, or times substantially greater than those observed. The source of the difference between measurements and predictions lies most likely in the use of diffusivities that describe solute transport through an annealed (unworked) β matrix. At warm processing temperatures, however, substantial dislocation substructure from prior warm working is likely retained in the β phase and thus enhances the kinetics due to pipe diffusion. The increase in diffusivity due to substructure developed during prior warm working is of the order of a factor of 10 [6]. Hence, the time to complete boundary grooving for the α lamellae would be ~20 h at 800 °C. This value is in reasonable agreement with the observed plateau (Fig. 9d), which may be associated with completion of the grooving process. In the case of annealing at 600 °C the corresponding adjustment to the diffusivity leads to a predicted time of ~1000 h, suggesting very slow kinetics, which is in broad agreement with the microstructural observations, i.e. microstructure evolution during deformation and subsequent annealing at 600 °C was associated primarily with spheroidization of the β phase rather than the α phase.

The model of fragmentation via boundary grooving is also applicable to the plate-like β phase, provided appropriate input data are available. However the tendency for β interlayers to fragment via thermal grooving during post-deformation heat treatment is lower than that for the α layers. This may be ascribed to two factors. First, the substructure in the β layers may be eliminated or the sub-boundary misorientation/energy may be rapidly reduced because of the rapid diffusion of vacancies in this phase. Second, the diffusion of solutes through the α phase (which may control the grooving kinetics of the β layers) is quite slow compared with the diffusion of solutes through the β phase (which appears to control grooving through the α phase) [31,32]. Even after accounting for the approximately fivefold difference in thickness between the α and β layers the time to complete grooving for the β phase would still be approximately 100 times longer than for the α phase. Therefore, fragmentation of the β layers may due to a gross geometric (thinning) phenomenon rather than thermal grooving per se.

3.5.2. Static spheroidization via termination migration

To interpret the post-boundary grooving behavior of α lamellae observed during long time annealing at 800 °C the time required for static spheroidization via termination migration was estimated using the equation [5,6]:

$$\frac{\tau_{vd}}{\tau'} = \frac{\eta^3 - \left[0.328\eta^{\frac{7}{3}}\left(1 + \sqrt{1 - 0.763\eta^{\frac{-4}{3}}}\right)^2\right]}{4\left[\frac{2(1+\eta)}{3\left(0.5 - 0.573\eta^{\frac{-1}{3}}\right)} + \frac{0.5\eta^{\frac{1}{3}} + 0.665\eta^{\frac{2}{3}}}{3\left(0.143 + 0.934\eta^{\frac{-1}{3}}\right)}\right]}, \tag{5}$$

Here, η is a geometric factor equal to $(w/d_\alpha) + 0.5$, in which w and d_α denote the initial diameter and the thickness of the pancake-shaped α particles, respectively. The time normalization factor τ' in the above relation is:

$$\tau' = \frac{d_\alpha^3 R_g T}{D_v^\beta C_\beta \gamma_{\alpha\beta} V_M}, \tag{6}$$

The input data for Eq. (6) are the same as in Section 3.5.1. Diffusivity was taken as $D_v^\beta = 0.0065\ \mu\text{m}^2\ \text{s}^{-1}$, assuming that dislocation substructure was eliminated in the material annealed for short times at 800 °C. The value of w at 800 °C was ~12 μm for a material predeformed at $\varepsilon = 0.69$ (Fig. 6b). The term C_β in Eq. (6) should be replaced by the composition factor $C_F \approx 14$ at 800 °C.

The calculated value for the spheroidization time by termination migration τ_{vd} was 104 h. This value of spheroidization time shows good agreement with the measured time of 50 h (Fig. 9d) to achieve approximately 80–90% spheroidization.

4. Conclusions

Evolution of the lamellar microstructure in Ti–6Al–4V alloy during working and subsequent annealing at 600 and 800 °C was investigated via isothermal compression testing. The features of microstructure evolution were found to be temperature dependent. The main conclusions from this work are as follows:

1. The stress–strain curves of the alloy compressed at 600 and 800 °C and a nominal strain rate of $10^{-3}\ \text{s}^{-1}$ exhibit an initial hardening transient, a peak flow stress, and then flow softening. Flow softening can be ascribed to rotation of lamellae towards "softer" orientations with low Taylor factors and evolution of the dislocation substructure.

2. Microstructure evolution during compression at both 600 and 800 °C comprised elongation of the β grains and rotation of the α lamellae towards the metal flow direction.
3. At 800 °C transformation of the lamellar microstrucuture into a globular one is controlled by fragmentation of α lamellae by the boundary splitting mechanism (associated with boundaries formed due to CDRX) and subsequent spheroidization of remnant α lamellae by means of termination migration.
4. A decrease in working temperature to 600 °C results in increased shear straining and a lower volume fraction of the β phase. Thin β layers transform relatively quickly into separate particles, while α becomes the matrix phase. Evolution of the microstructure of the α phase is associated with CDRX (during deformation) and possibly static recrystallization within each phase during subsequent annealing.

Acknowledgment

This work was supported by the Federal Agency for Education, Russia, Grant no. P2486.

References

[1] Leyens C, Peters M. Titanium and titanium alloys. Fundamentals and applications. Weinheim: Wiley-VCH; 2003.
[2] Tian YL, Kraft RW. Metall Trans A 1987;18:1403.
[3] Stefansson N, Semiatin SL. Metall Mater Trans A 2003;34:691.
[4] Sharma G, Ramanujan RV, Tiwari GP. Acta Mater 2000;48:875.
[5] Semiatin SL, Stefansson N, Doherty RD. Metall Mater Trans A 2005;6:1372.
[6] Semiatin SL, Furrer DU. Modeling of microstructure evolution during the thermomechanical processing of titanium alloys. In: Semiatin SL, Furrer DU, editors. ASM Handbook, vol. 22. Fundamentals of Modeling for Metals Processing. Materials Park, OH: ASM International; 2009.
[7] Mullins WW. J Appl Phys 1957;28:333.
[8] Nakagawa YG, Weatherly GC, Ho E. Trans JIM 1974;15:114.
[9] Dahmen U. Acta Metall 1982;30:63.
[10] Furuhara T, Ogawa T, Maki T. Philos Mag Lett 1995;72:175.
[11] Mazurski MI, Salishchev GA. Phys Status Solidi B 1995;187:501.
[12] Zherebtsov S, Salishchev G, Semiatin SL. Philos Mag Lett 2010;90:903.
[13] Zherebtsov S, Mironov S, Murzinova M, Salishchev G, Semiatin SL. Mater Sci Forum 2008;584–586:771.
[14] Weiss I, Froes FH, Eylon D, Welsch GE. Metall Trans A 1986;17:1935.
[15] Meyers MA, Chawla KK. Mechanical behavior of materials. New York: Cambridge University Press; 2009.
[16] Humphreys F, Hatherly M. Recrystallization and related annealing phenomena. Oxford: Elsevier; 2004.
[17] Zherebtsov SV, Salishchev GA, Galeyev RM, Valiakhmetov OR, Mironov S Yu, Semiatin SL. Scripta Mater 2004;51:1147.
[18] Semiatin SL, Seetharaman V, Weiss I. Mater Sci Eng A 1999;263:257.
[19] Stefansson N, Semiatin SL, Eylon D. Metall Mater Trans A 2002;33:3527.
[20] Miller RM, Bieler TR, Semiatin SL. Scripta Mater 1999;40:1387.
[21] Suri S, Viswanathan GB, Neeraj T, Hou D-H, Mills MJ. Acta Mater 1999;47:1019.
[22] Mironov S, Murzinova M, Zherebtsov S, Salishchev GA, Semiatin SL. Acta Mater 2009;57:2470.
[23] Gundersen HJG, Jensen TB, Osterby RJ. Microscopy 1977;113:27.
[24] Semiatin SL, Montheillet F, Shen G, Jonas JJ. Metall Mater Trans A 2002;33:2719.
[25] Sargent GA, Zane AP, Fagin PN, Ghosh AK, Semiatin SL. Metall Mater Trans A 2008;39:2949.
[26] Mullins WW. Trans Metall Soc AIME 1960;218:354.
[27] Read WT, Shockley W. Phys Rev 1950;78:275.
[28] Martin JW, Doherty RD, Cantor B. Stability of microstructure in metallic systems. Cambridge: Cambridge University Press; 1997.
[29] Semiatin SL, Kirby BC, Salishchev GA. Metall Mater Trans A 2004;35:2809.
[30] Semiatin SL, Knisley SL, Fagin PN, Zhang F, Barker DR. Metall Mater Trans A 2003;34:2377.
[31] Liu Z, Welsch G. Metall Trans A 1988;19:1121.
[32] Mishin Y, Herzig C. Acta Mater 2000;48:589.